Comprehensive power loss modelling to improve the performance of an Energy Recovery Station for water utility networks

Loïc Andolfatto[1], *Head of Laboratory for Hydraulic Machines Testing Team*, loic.andolfatto@epfl.ch
Daniel Biner[2], *Scientific assistant*
Cécile Münch-Alligné[2], *Head of the research group "Hydroelectricity"*
François Avellan[1], *Director of Laboratory for Hydraulic Machines*

[1]École polytechnique fédérale de Lausanne, Laboratory for Hydraulic Machines
Avenue de Cour 33 bis, 1007 Lausanne, Switzerland

[2]University of Applied Sciences Western Switzerland, HES-SO Valais-Wallis
Route du Rawyl 47, 1950 Sion 2, Switzerland

Abstract

The work presented in this paper details the methodology applied to inventory and estimate the power losses in a micro-turbine with counter-rotating runners. The separation between the impact of design parameters and operational parameters on each identified source of power loss provides an efficient framework for optimal design of a family range of standard turbines. The qualitative inventory can be used at early stage of the design for specification purpose while the quantitative aspect can serve for optimizing the system accounting for all the loss sources.

1. Introduction

Beside large hydropower schemes, the increase of sustainable hydraulic energy production also rely on the development of new technologies dedicated to harvesting the small-scale hydroelectric potential. For instance, the Swiss yearly small hydropower production – generated on stations with a nominal power below 300 kW – is expected to grow from 0.3 TWh to 1.3 TWh between 2010 and 2050 as stated [1]. Several examples of successful implementations of conventional hydraulic machines technologies (Pelton turbine, Francis turbine, pump as turbines, etc.) to recover hydropower potential on drinking water networks are exposed in [2]. These conventional technologies applied to small hydropower face either a high capital expenditure or limited performance under the fluctuating discharge conditions commonly experienced on consumption-driven networks.

The concept of modular Energy Recovery Station [3], illustrated in Figure 1 and Figure 2, has been developed to overcome the difficulties encountered when harvesting hydropower on existing infrastructures in the 5 kW to 25 kW power range. It features an axial micro-turbine with counter-rotating runners for in-line installation [4,5] limiting the infrastructure modifications for its installation. The hydraulic design has been investigated both numerically [6] and experimentally [7]. The micro-turbine has two runners with a fixed geometry operated with independent variable speed. The wide operating range offered by the double regulation, similar to other double-regulated turbines, is adapted to the consumer-driven discharge fluctuation experienced on drinking water network. A dedicated sensor less control strategy allows to operate on-cam across this wide operating range while limiting the cost of embedded instrumentation [8,9].

1

In order to provide a framework for optimal design of a family range of energy recovery station addressing the various operating conditions existing in drinking water infrastructures, this paper presents a comprehensive inventory of power losses sources in the micro-turbine associated with quantitative models. For power loss sources for which the magnitude depends on choice made during the mechanical design phase, a model of the power loss as a function of the operating conditions is proposed, to finally plot a power loss hill chart in section 5.
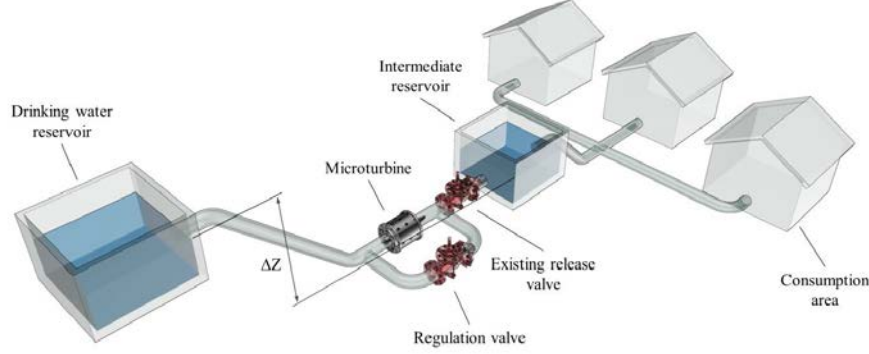

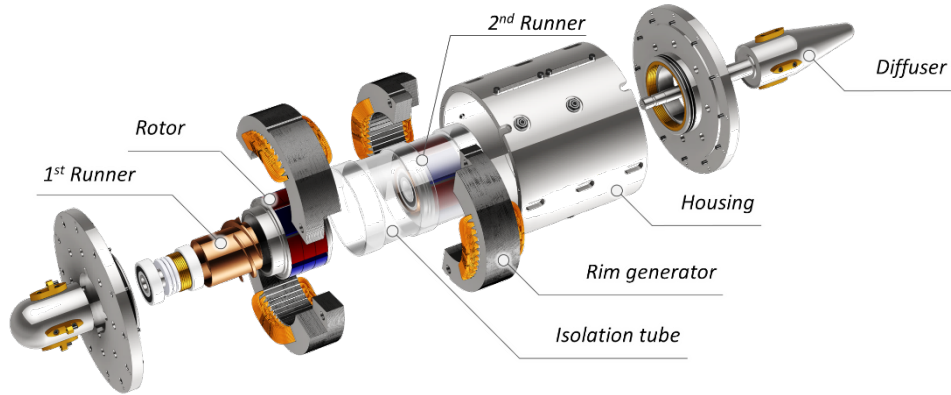*Figure 1: Layout of a drinking water system with integrated micro-turbine [5].*

Figure 2: Single-stage architecture of the DuoTurbo concept with integrated generators.

2. General assumptions and hypothesis

The system considered in this paper is the DuoTurbo Prototype V0 described in [5] The mapping of the power losses is conducted on the operating domain of the system defined according to the on-cam points identified during the experimental campaign. Each point is defined by the following quantities:

- the discharge Q passing through the turbine;
- the difference of specific energy E between the inlet and the outlet of the turbine;
- the rotational speed N_A of the first runner;
- the rotational speed N_B of the second runner.

For each point of the operating domain, the values of the following quantities have been measured or computed:

-   the hydraulic power P_h is computed according to (1), with ρ the density of the water;

$$P_h = \rho \cdot Q \cdot E \tag{1}$$

-   the output power P is computed according to (2) with P_A and P_B being the output power measured from the first and second runner respectively;

$$P = P_A + P_B \tag{2}$$

-   the efficiency η is computed according to (3).

$$\eta = \frac{P}{P_h} \tag{3}$$

-   the torques T_A and T_B transmitted to the first and second generators are given by:

$$T_i = \frac{P_i}{\omega_i} = \frac{30 \cdot P_i}{\pi \cdot N_i} \tag{4}$$

3. Power losses inventory

3.1. Power balance equation

The power losses in the system are classified in 4 categories:

-   volumetric losses P_{rq} due to leakage out of the hydraulic section of the runner;
-   hydraulic losses P_{rh} due to the flow power dissipation;
-   friction losses P_{rm} due to friction between moving components;
-   electrical losses P_{rel} due to losses in the conversion of mechanical power into electrical power.

The power balance equation (5) is illustrated by the power losses cascade in Figure 3.
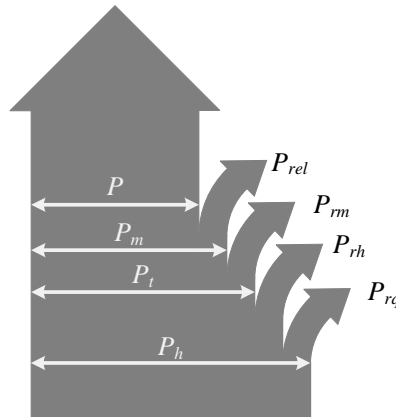
$$P = P_h - (P_{rq} + P_{rh} + P_{rm} + P_{rel}) \tag{5}$$

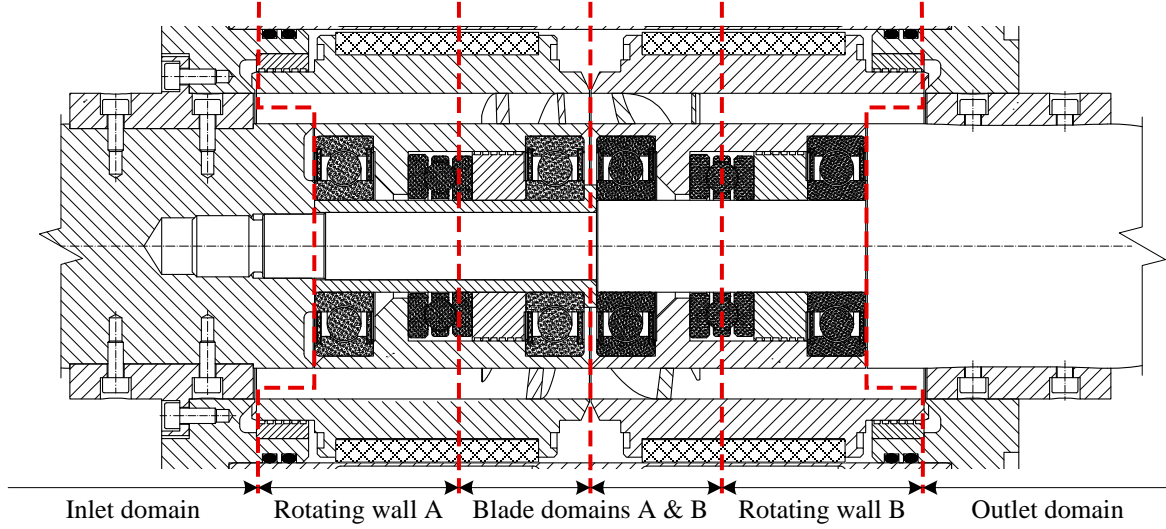*Figure 3: Representation of the power losses cascade between hydraulic and output power.*

| Inlet domain | Rotating wall A | Blade domains A & B | Rotating wall B | Outlet domain |

Figure 4: Decomposition of the hydraulic passage of the micro-turbine into 6 regions.

3.2. Detailed power losses inventory

3.2.1. Volumetric losses

Leakages are experienced within the hub and around the shroud of each runner, represented by the elementary power loss contributors $P_{rq,hA}$, $P_{rq,hB}$, $P_{rq,sA}$, $P_{rq,sB}$, standing for hub and shroud and first and second runner respectively. The operating parameter influencing these contributors is the specific energy E extracted by the turbine. They also depend on the technical choices made for the design of the seals.

3.2.2. Hydraulic losses

The hydraulic passage of the micro-turbine is arbitrarily decomposed into 6 domains defined in Figure 4. The flow power dissipations in the inlet domain and in the outlet domain are not considered. The decomposition along each runner into a rotating wall domain and a blade domain is proposed in order to decompose the dissipations due to the hydraulic design of the runner on one hand and the dissipations due to the mechanical design, such as the length of the rotating wall from the hub and from the shroud.

The losses in the blade domains are referred to as $P_{rh,A}$ and $P_{rh,B}$. In the following, the losses $P_{rh,wA}$ and $P_{rh,wB}$ .in the rotating wall domains of runners A and B respectively are assumed to depend on the length of the walls and the hub and shroud radius set during the design. The operating parameters with an influence on these loss contributors are the rotational speed N and the mean flow velocity depending on the discharge Q.

3.2.3. Friction losses

Friction loss sources due to direct contact between components and viscous friction in thin fluid layers are separated in two categories.

Firstly, direct friction between components in physical contact with relative motion are considered with $P_{rm,bA}$ and $P_{rm,bB}$ standing for the losses in the bearing of runner A and runner B respectively. The technical choices selected for the bearing have a direct influence on the magnitude of these losses. The driving operating parameters are the rotational speed N and the axial thrust supported by the bearing that depends on the specific energy E extracted by the turbine and by several dimensions defined during the detailed mechanical design phase.

Secondly, power dissipations in the water layer between components separated by a thin fluid layer and with relative motion are also considered as viscous friction losses. This situation is encountered at the gap in hub and shroud labyrinth seals of both runners, leading to the inventory of $P_{rm,hA}$, $P_{rm,sA}$, $P_{rm,hB}$ and $P_{rm,sB}$. The reduced gap between the rotors and the isolation polymer tube is also a source of friction power losses referred to as $P_{rm,gA}$ and $P_{rm,gB}$. These loss contributors directly depend on the dimensions of the component defined at the detailed mechanical design stage. The driving operating parameter is the rotational speed N.

3.2.4. *Electrical losses*

The electrical losses are decomposed into two separate categories: Joules losses and other electromagnetic losses. The Joule losses $P_{rel,JA}$ and $P_{rel,JB}$, in generators A and B respectively, depend on the air gap between the rotor and the stator of the generator. The driving operating parameter is the torque T. The other electromagnetic losses $P_{rel,emA}$ and $P_{rel,emB}$ in generators A and B are assumed to be independent from the mechanical design. They are not considered any further in this paper.
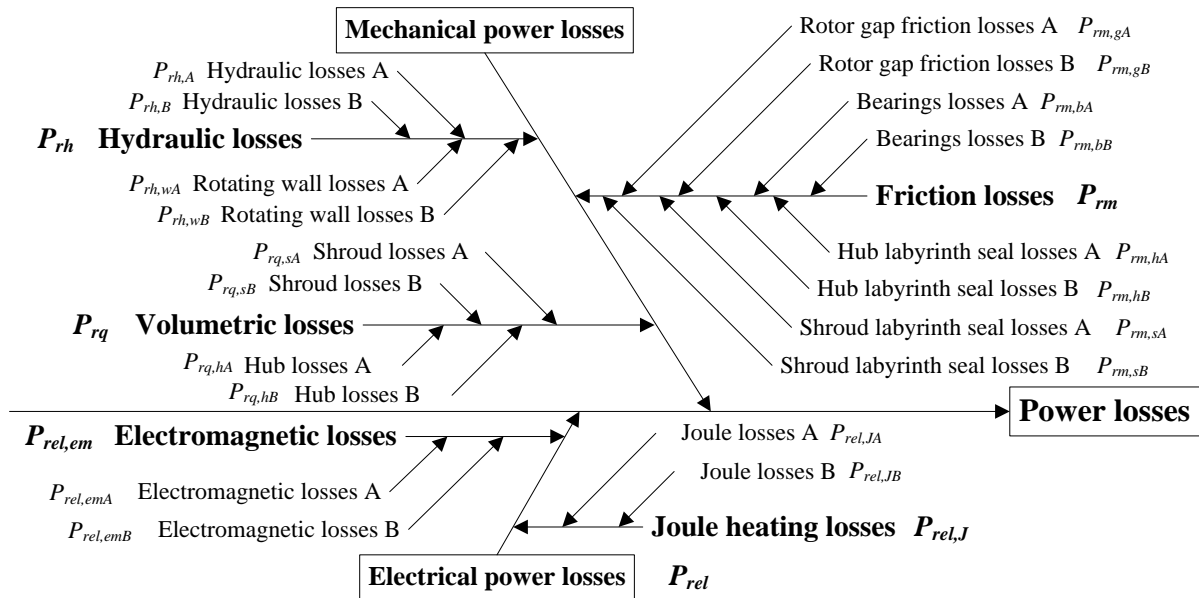

Figure 5: Detailed power losses inventory represented in an Ishikawa diagram.

5

3.2.5. *Synthesis*

A classified inventory of the identified and defined power loss contributors is graphically represented in Figure 5. For these contributors, the operating parameters influencing the magnitude of the power loss are also identified in Table 1.

Table 1: Power losses inventory with driving operating parameters

| Power loss contributor	Symbol	Operating parameter
Hub volumetric losses A	$P_{rq,hA}$	E
Hub volumetric losses B	$P_{rq,hB}$	E
Shroud volumetric losses A	$P_{rq,sA}$	E
Shroud volumetric losses B	$P_{rq,sB}$	E
Flow power dissipation in runner A blade domain	$P_{rh,A}$	Q, E
Flow power dissipation in runner B blade domain	$P_{rh,B}$	Q, E
Flow power dissipation in rotating wall domain A	$P_{rh,wA}$	N, Q
Flow power dissipation in rotating wall domain B	$P_{rh,wB}$	N, Q
Mechanical friction losses in runner A bearing	$P_{rm,bA}$	N, E
Mechanical friction losses in runner B bearing	$P_{rm,bB}$	N, E
Viscous friction losses in runner A hub labyrinth seal	$P_{rm,hA}$	N
Viscous friction losses in runner B hub labyrinth seal	$P_{rm,hB}$	N
Viscous friction losses in runner A shroud labyrinth seal	$P_{rm,sA}$	N
Viscous friction losses in runner B shroud labyrinth seal	$P_{rm,sB}$	N
Viscous friction losses in runner A rotor vs. tube gap	$P_{rm,gA}$	N
Viscous friction losses in runner B rotor vs. tube gap	$P_{rm,gB}$	N
Joule heating losses in generator A	$P_{rel,JA}$	T
Joule heating losses in generator B	$P_{rel,JB}$	T
Electromagnetic losses in generator A	$P_{rel,emA}$	T, N
Electromagnetic losses in generator B	$P_{rel,emB}$	T, N
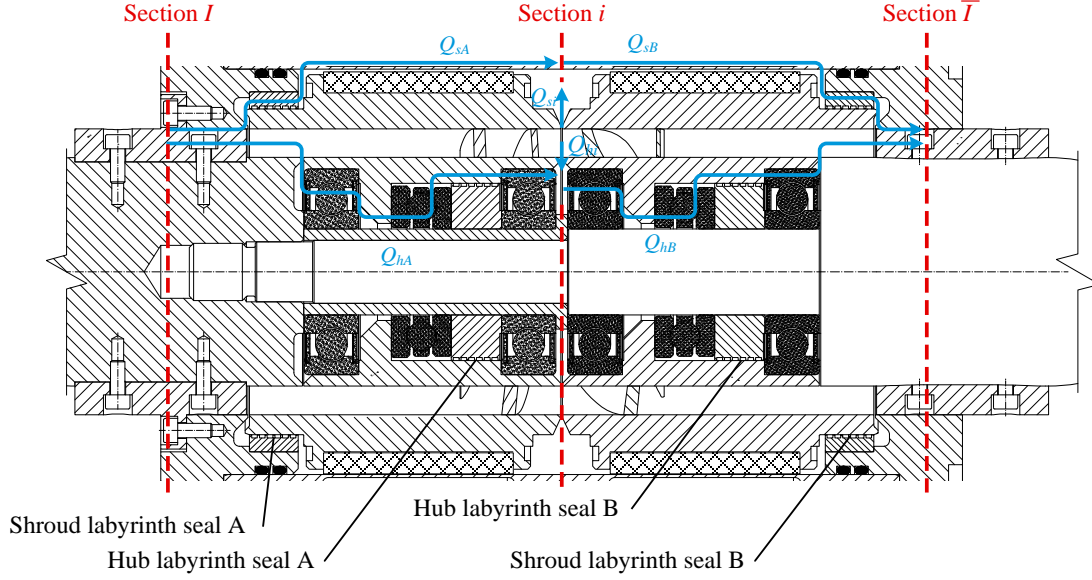
Figure 6: Secondary discharges between the three identified sections of the turbine.

4. Modelling of the power losses

4.1. Parametric power loss models

4.1.1. Volumetric losses

Leaking flows circulating inside the hub our outside the shroud are depicted in Figure 6. The convention for positive values of the discharge are defined according to the arrows representing the flows. Each volumetric power losses $P_{r,k}$ is computed according to (6).

$$P_{r,k} = \rho \cdot Q_{rq,k} \cdot E_k \tag{6}$$

The schematic representation of Figure 7 provides a schematic representation of the system supporting the formulation of the problem. The leaking discharges are obtained by writing mass balance equations in section I and section $\overline{I}$ inside hub and outside shroud:

$$\begin{cases} Q_{rq,sA} = Q_{sA} \\ Q_{rq,hA} = Q_{hA} \\ Q_{rq,sB} = Q_{sB} + Q_{si} \\ Q_{rq,hB} = Q_{hB} + Q_{hi} \end{cases} \tag{7}$$

The system (7) features 6 unknowns. Its resolution requires to write 6 energy balance equations. The difference of specific energy at the bounds of each channel depends on its equivalent energy loss coefficient $k_{eq,j}$ and follows the generic law formulated in (8).

$$E_j = k_{eq,j} \cdot \frac{Q_k \cdot |Q_k|}{2} \tag{8}$$

7

The energy balance equations formulated according to are given in the system (9), with gH_u the specific energy in the section u.

$$
\begin{cases}
gH_I - gH_i = k_{eq,sA} \cdot \dfrac{Q_{sA} \cdot |Q_{sA}|}{2} - k_{eq,si} \cdot \dfrac{Q_{si} \cdot |Q_{si}|}{2} \\[2mm]
gH_I - gH_i = k_{eq,hA} \cdot \dfrac{Q_{hA} \cdot |Q_{hA}|}{2} - k_{eq,hi} \cdot \dfrac{Q_{hi} \cdot |Q_{hi}|}{2} \\[2mm]
gH_i - gH_{\bar{I}} = k_{eq,si} \cdot \dfrac{Q_{si} \cdot |Q_{si}|}{2} + k_{eq,sB} \cdot \dfrac{Q_{sB} \cdot |Q_{sB}|}{2} \\[2mm]
gH_i - gH_{\bar{I}} = k_{eq,si} \cdot \dfrac{Q_{si} \cdot |Q_{si}|}{2} + k_{eq,sA} \cdot \dfrac{Q_{sA} \cdot |Q_{sA}|}{2} \\[2mm]
gH_I - gH_{\bar{I}} = k_{eq,sA} \cdot \dfrac{Q_{sA} \cdot |Q_{sA}|}{2} + k_{eq,sB} \cdot \dfrac{Q_{sB} \cdot |Q_{sB}|}{2} \\[2mm]
gH_I - gH_{\bar{I}} = k_{eq,hA} \cdot \dfrac{Q_{hA} \cdot |Q_{hA}|}{2} + k_{eq,hB} \cdot \dfrac{Q_{hB} \cdot |Q_{hB}|}{2}
\end{cases}
\tag{9}
$$

For each channel, the equivalent energy loss coefficient $k_{eq,j}$ depends on its architecture and on the values of the design parameters. The nomenclature of design parameters related to labyrinth seals is provided in Figure 8. The design parameters related to the rotor are defined in Figure 9.

Regarding the secondary discharge in the shrouds, it encounters the energy losses in the labyrinth seal and the energy losses due to the restricted section between the rotor and the isolation polymer tube. Following the basic loss models for regular losses, sudden enlargement and sudden contraction of a flow, the equivalent loss coefficient is modelled by:

$$
k_{eq,sA} = k_{eq,sB} = \frac{1}{A_s^{\,2}} \left[\frac{3}{2} + z_g \left(1 - \frac{A_s}{A_{es}} \right)^2 + \lambda \frac{(z_g + 1)L_s}{2 j_{lab}} \right] + \frac{1}{A_r^{\,2}} \left[\frac{3}{2} + \frac{\lambda \cdot L_{rotor}}{2 (R_{tube} - R_{rotor})} \right]
\tag{10}
$$

with z_g the number of grooves in the labyrinth, λ the local loss coefficient depending on the Reynolds number in the considered area assuming a sand roughness of 1 µm and considering the Churchill formula. The reference sections are detailed in (11).

$$
\begin{cases}
A_s = \pi \left((R_e + j_{lab})^2 - R_e^2 \right) \\[2mm]
A_{es} = \pi \left((R_e + j_{lab} + e_{lab})^2 - R_e^2 \right) \\[2mm]
A_r = \pi \left(R_{tube}^2 - R_{rotor}^2 \right)
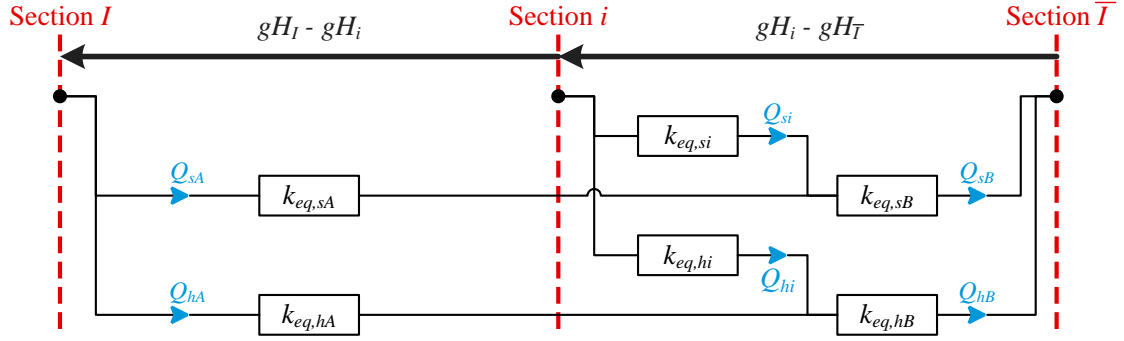\end{cases}
\tag{11}
$$

Figure 7: Schematic model of the secondary discharges
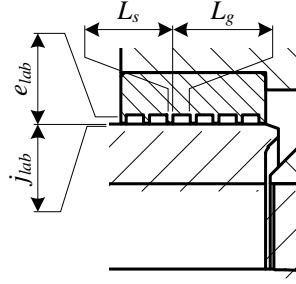

Figure 8: Labyrinth seal geometrical design parameters.
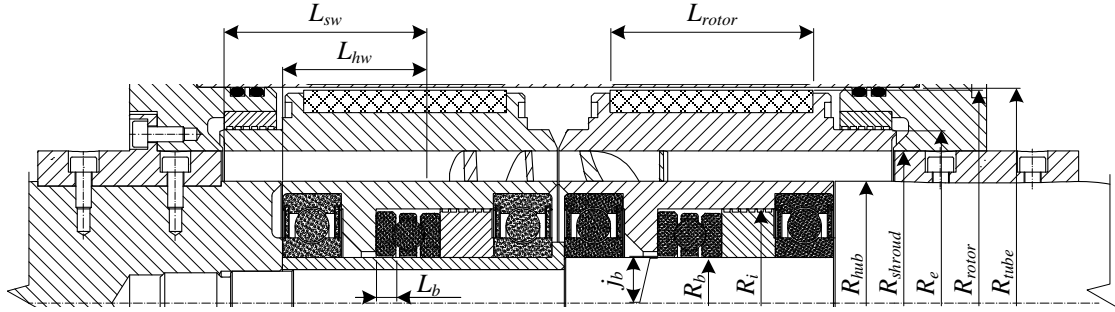

Figure 9: Design parameters of the rotors

For the secondary discharge inside the hub, it encounters the specific energy losses due to the restricted section between the fixed shaft and the rotating ring of the thrust bearing and the specific energy losses in the labyrinth seals. The equivalent loss coefficient is given by (12) with the reference section taken from (13).

$$k_{eq,hA} = k_{eq,hB} = \frac{1}{A_h^2}\left[\frac{3}{2} + z_g\left(1 - \frac{A_h}{A_{eh}}\right)^2 + \lambda\frac{(z_g+1)L_s}{2j_{lab}}\right] + \frac{1}{A_b^2}\left[\frac{3}{2} + \frac{\lambda \cdot L_b}{2 \cdot j_b}\right] \tag{12}$$

$$\begin{cases} A_h = \pi \left(R_i^2 - \left(R_i - j_{lab} \right)^2 \right) \\ A_{eh} = \pi \left(R_i^2 - \left(R_i - j_{lab} - e_{lab} \right)^2 \right) \\ A_b = \pi \left(\left(R_b + j_b \right)^2 - R_b^2 \right) \end{cases} \qquad (13)$$

Finally, the discharges in the inter-runner section Q_{si} and Q_{hi} are expected to be small compared to the other secondary discharges and the available section is big compared to other sections. It leads to small flow velocities and therefore negligible energy losses. The associated equivalent loss coefficients are then assumed to equal 0 in the following. As the regular loss coefficients λ depends on the flow velocity, the non-linear system (9) is solved iteratively.

The specific energy level in section i is not measured during the experimental campaign. Therefore, the assumption is made that the dispatch of the specific energy between the two runners is proportional to the dispatch of the output power as in (14).

$$\frac{E_A}{E_B} = \frac{gH_I - gH_i}{gH_i - gH_{\bar{I}}} = \frac{P_A}{P_B} \qquad (14)$$

4.1.2. *Hydraulic losses in the rotating wall domains*

The two design parameters integrated in the parametric model of the hydraulic losses in the rotating wall domains are the length of the wall included in the rotating wall domains at the shroud and at the hub, L_{sw} and L_{hw} respectively as illustrated in Figure 9. The model used for the hydraulic power losses in the rotating wall domain is expressed in (15).

$$P_{rh,w} = \left[\begin{pmatrix} 1 & \omega & Q & \omega^2 & \omega Q & Q^2 \end{pmatrix} \cdot \left[C_s \cdot \begin{pmatrix} 1 \\ L_{sw} \\ L_{sw}^2 \end{pmatrix} + C_h \cdot \begin{pmatrix} 1 \\ L_{hw} \\ L_{hw}^2 \end{pmatrix} \right] \right] \cdot \omega \qquad (15)$$

The two pseudo-matrix C_s and C_h are identified from a set of numerical simulations. Their values depend on the shroud and hub radius R_{shroud} and R_{hub} respectively.

4.1.3. *Mechanical friction losses*

The mechanical friction losses model expressed in (16) is adapted from [10], with f the equivalent friction coefficient of the bearing, D its equivalent diameter, with values of 0.013 and 60 mm respectively, both taken from tables in [10].

$$P_{rm,m} = f \cdot D \cdot F \cdot \omega \qquad (16)$$

Regarding the equivalent mechanical solicitation F, it is assumed to be purely axial force as the only radial forces are the rotor own weight and the electromagnetic force from the rotor-stator interaction; both at least one order of magnitude less than the axial force. Thus, it directly depends on the specific energy extracted by the runner and on the area exposed to the associated difference of pressure. The mechanical friction losses model for the runner X is finally given by:

10

$$P_{rm,bX} = f \cdot D \cdot \left(\rho \cdot E_X \cdot \pi \left(R_e^2 - R_i^2 \right) \right) \cdot \omega_X \tag{17}$$

As the mechanical system is highly over constrained and as it is operating in water while tables provides f for operation in lubricated conditions, these contributors to power losses are likely to be underestimated.

4.1.4. *Viscous friction losses*

The power dissipated by viscous friction between two cylinders of length L and radius R_{ext} and R_{int} rotating with a relative rotational speed ω in a fluid of dynamic viscosity μ is expressed in (18).

$$P_{rmv} = 4 \cdot \pi \cdot \mu \cdot L \frac{R_{ext}^2 \cdot R_{int}^2}{R_{ext}^2 - R_{int}^2} \cdot \omega^2 \tag{18}$$

The design parameters influencing the power loss contributors previously identified are summarized in Table 2.

Table 2: Design parameters influencing the viscous friction power losses

Power loss contributor	Symbols	Length	External radius	Internal radius
Hub labyrinth seal	$P_{rm,hA}, P_{rm,hB}$	$\left(z_g + 1 \right) L_s$	$R_e + j_{lab}$	R_e
Shroud labyrinth seal	$P_{rm,sA}, P_{rm,sB}$	$\left(z_g + 1 \right) L_s$	R_i	$R_i - j_{lab}$
Rotor vs. tube gap	$P_{rm,gA}, P_{rm,gB}$	L_{rotor}	R_{tube}	R_{rotor}

4.1.5. *Joule losses*

The Joule power losses is assumed to be proportional to the squared torque, with a Joule loss factor that depends on the air gap j_G between the permanent magnets and the stator. The final Joule Losses model expressed in (19) is identified according to numerical simulation presented in [5].

$$P_{rel,J} = \left(-29702 \cdot j_G^2 + 362.2 \cdot j_G - 0.17898 \right) \cdot T^2 \tag{19}$$

The curve fitting is performed on the available dataset going from 2.9 mm to 5 mm. Thus, the validity of this model is not necessarily covering this entire range and air gap values higher than 4 mm may lead to underestimated power losses.

4.2. Non-parametric power loss models

4.2.1. Electromagnetic losses

Considering the Joule loss model proposed in the previous section and the efficiency map of the generators taken from [5], a parametric model of the residual losses is identified and proposed in (20) according to reduced operating conditions N^* and T^* following (21).

$$P_{rel,em} = 123 + 59.7\, N^* + 7.552 T^* + 5.94\, \frac{\sqrt{2}}{2}\left(N^{*2} - 1\right) + N^* T^* - 3.33\frac{\sqrt{2}}{2}\left(T^{*2} - 1\right) \qquad (20)$$

$$\begin{cases} N^* = \dfrac{N - 2250}{861.9} \\ T^* = \dfrac{T - 6}{2.60} \end{cases} \qquad (21)$$

4.2.2. Hydraulic losses

Hydraulic losses in the blade domain are estimated according to a polynomial chaos model identified with the method described in [8] applied on a data set generated through CFD numerical simulations.

5. Quantitative analysis

According to the presented models, a quantitative analysis of the losses can be performed for any point of the operating domain. An example is provided at the point described on the efficiency hill chart of Figure 10. The value of the power loss contributions at this operating point are summarized in Table 3 and in Figure 11.

The power loss contributions over the entire operating domain is represented in Figure 12. Such graphical representation is powerful to understand the respective evolutions of each contributors and their effect on the global performance of the designed unit.

Table 3: Power losses contributions for the example operating point.

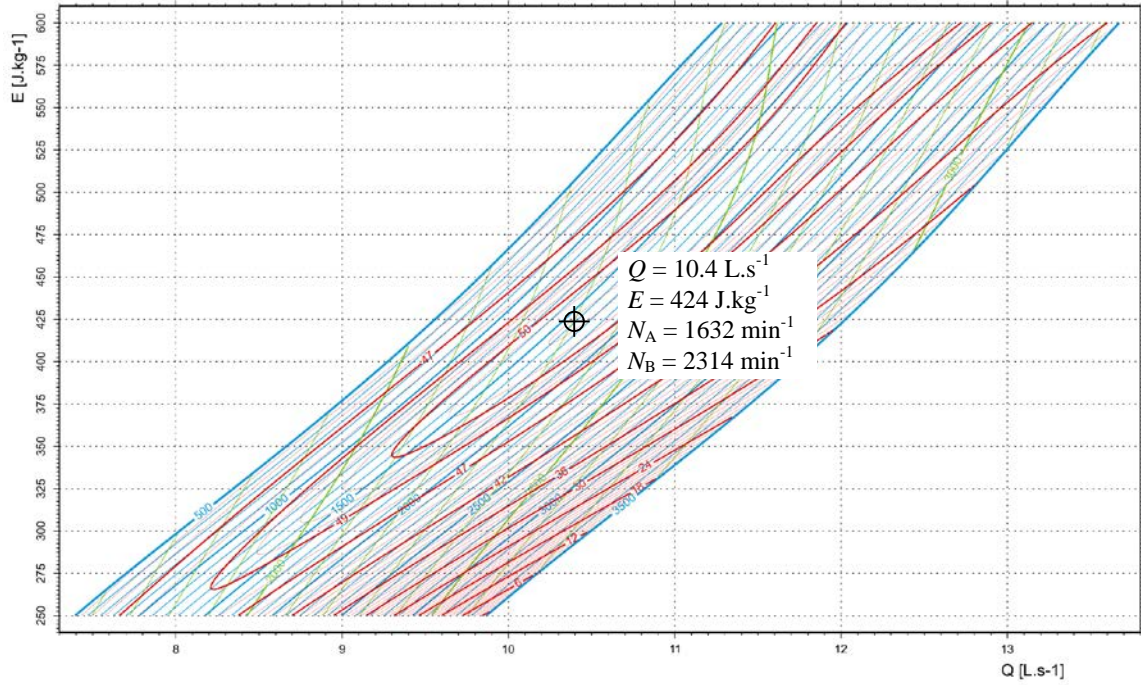| Power loss contributor	Value [W]
Volumetric losses	191
Hydraulic losses in rotating wall domains	149
Friction losses in bearings	314
Friction losses in seals	6
Friction losses in rotor vs. tube gap	35
Joule heating losses	36
Electromagnetic losses	204

Figure 10: Example operating point on the efficiency hill chart identified during the test campaign of January 2016.
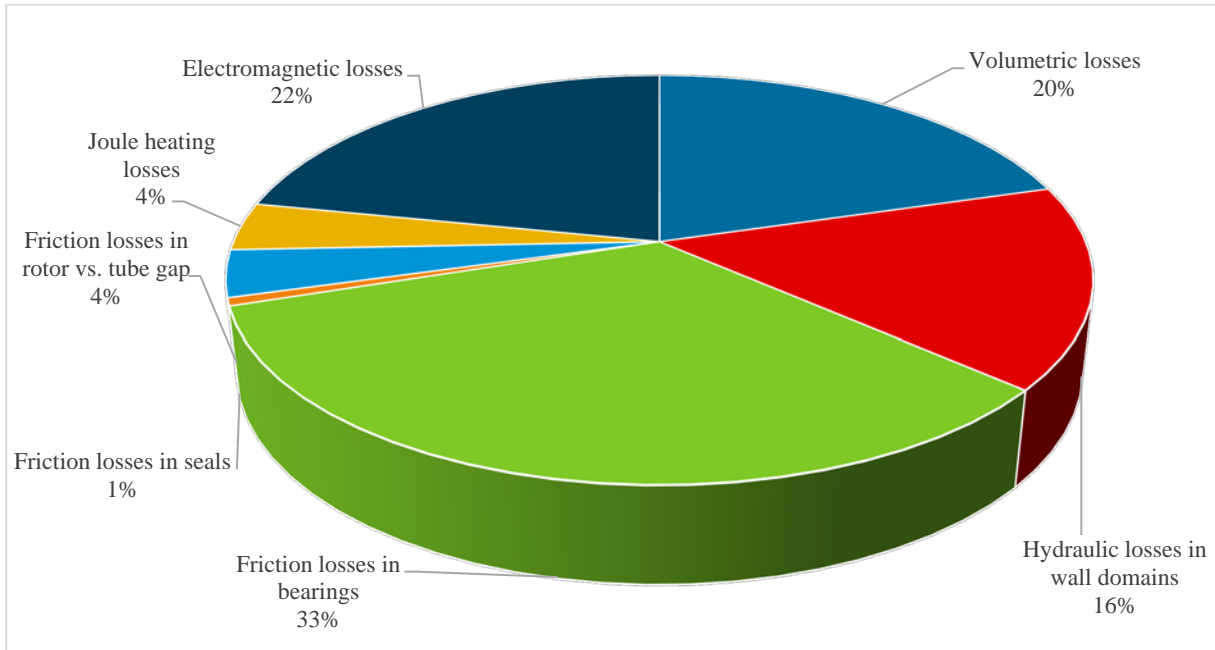

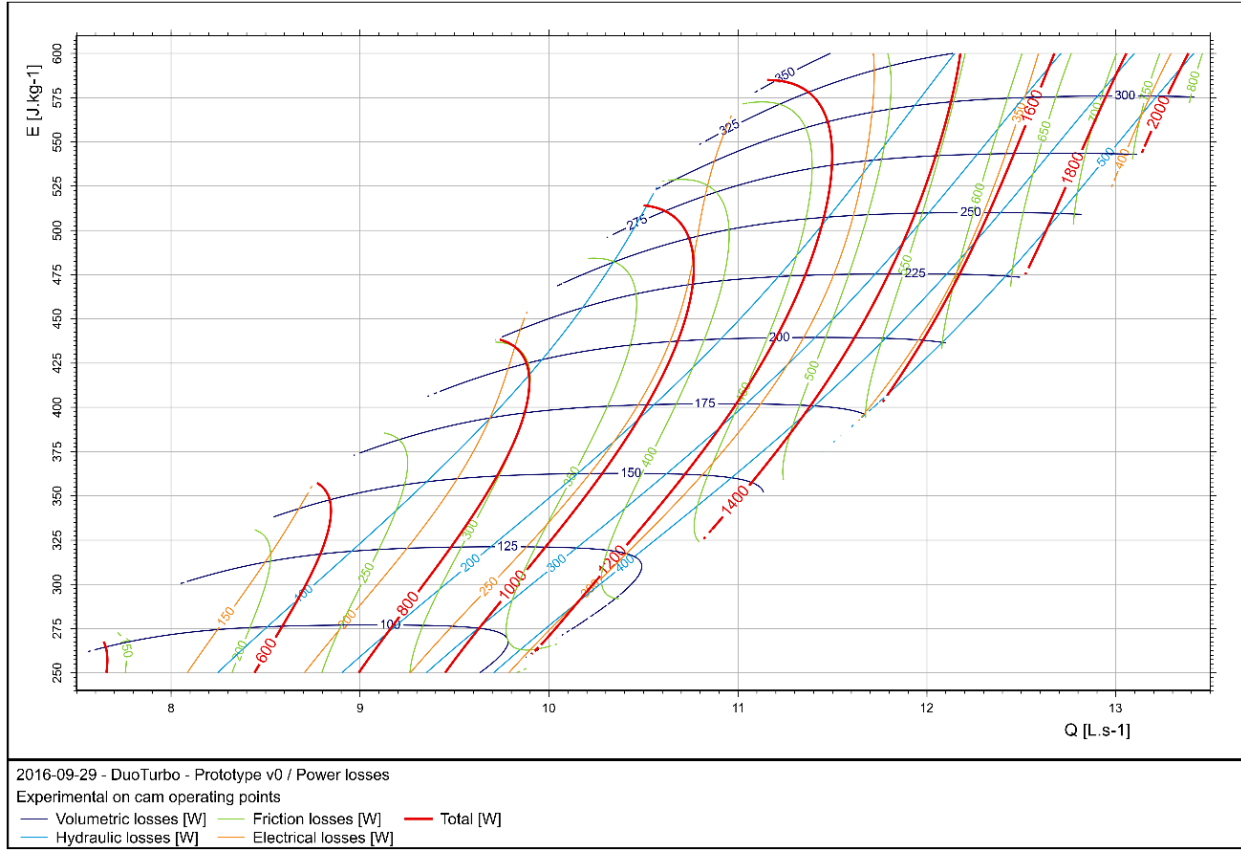*Figure 11: Graphical representation of the modeled power losses with relative contribution to the total losses.*

Figure 12: Power losses hill chart according to the proposed models

6. Conclusion

The work presented in this paper aims at providing a qualitative and quantitative analysis of the power losses in the electro-mechanical part of an Energy Recovery Station featuring a micro-turbine with counter-rotating runners and embedded permanent magnets synchronous generators.

From the methodological point of view, the inventory of power losses based on the power balance equation established in section 3 is applicable to the engineering of any hydraulic machine. The identification of the influencing operating parameters on the power loss sources is one of the drivers for the specification of a modular family range of components for the Energy Recovery Stations and the selection of technical solutions.

The modelling of the power losses as functions of the design parameters and operating parameters developed in section 0 is a powerful and effective method for quantitative analysis. Even if the models are highly linked to the technical choices made during the design process, it allows optimizing the losses over of the entire system. This is particularly effective when some design parameters, such as the gap j_G between the stator and the rotor, are involved in several contributors to the losses, *e.g.* viscous friction losses and Joule losses.

Finally, the quantitative analysis presented in section 5 allows identifying and comparing the respective impact of each source of power losses. The engineering of small hydropower units in

14

the kilowatt range requires tradeoff between the energetic performance achieved by the units and the costs and efforts undertaken for their design and their manufacturing. In that context, having the ability to identify quickly and to focus on the critical elements of the design is one of the key elements towards a successful techno-economic development of Energy Recovery Station. The work presented in this paper is directly serving this goal.

7. Acknowledgment

References

[1] Swiss Academy of Engineering Sciences (SATW) (2006). Road Map - Renewable Energies Switzerland - An analysis with a view to harnessing existing potentials by 2050. http://www.satw.ch/publikationen/schriften/39_roadmap_e.pdf

[2] Bühler, T. (2007). Turbinage dans les réseaux d'eau. *Gas, Wasser, Abwasser (GWA)* 6, 435-440.

[3] Andolfatto, L.; Euzenat, C.; Vagnoni, E.; Münch-Aligné, C. & Avellan, F. A mixed standard/custom design strategy to minimize cost and maximize efficiency for picohydro power potential harvesting *5th International Youth Conference on Energy (IYCE)*, Pisa, Italy, 2015, DOI: 10.1109/IYCE.2015.7180729

[4] Biner, D.; Hasmatuchi, V.; Avellan, F. & Münch-Alligné, C. Design and performance of a hydraulic micro-turbine with counter-rotating runners, *5th International Youth Conference on Energy (IYCE),* Pisa, Italy, 2015, 1-10, DOI: 10.1109/IYCE.2015.7180737

[5] Biner, D.; Hasmatuchi, V.; Violante, D.; Richard, S.; Chevailler, S.; Andolfatto, L.; Avellan, F. & Münch, C. Engineering and Performance of DuoTurbo: Microturbine with Counter-Rotating Runners *28th IAHR symposium on Hydraulic Machinery and Systems*, July 4-8th, Grenoble, France, 2016, DOI: 10.1088/1755-1315/49/10/102013

[6] Münch-Alligné, C.; Richard, S.; Meier, B.; Hasmatuchi, V. & Avellan, F. Numerical Simulations of a Counter-Rotating Micro-Turbine. *Advances in Hydroinformatics*, Springer Singapore, 2014, 363-373, DOI: 10.1007/978-981-4451-42-0_30

[7] Vagnoni, E.; Andolfatto, L.; Delgado, J.; Münch-Alligné, C. & Avellan, F. Application of Laser Doppler Velocimetry to the development of a counter rotating micro-turbine. *36th IAHR World Congress*, The Hague, The Netherlands, 2015

[8]   Andolfatto, L.; Delgado, J.; Vagnoni, E.; Münch-Aligné, C. & Avellan, F. Analytical hill chart towards the maximisation of energy recovery on water utility networks with counter rotating micro-turbine *36th IAHR World Congress*, The Hague, The Netherlands, 2015

[9]   Andolfatto, L.; Vagnoni, E.; Hasmatuchi, V.; Münch-Alligné, C. & Avellan, F. Simulation of energy recovery on water utility networks by a micro-turbine with counter-rotating runners. *28th IAHR symposium on Hydraulic Machinery and Systems,* July 4-8th, Grenoble, France, 2016, DOI: 10.1088/1755-1315/49/10/102012

[10] J.-L. Fanchon, Guide des sciences et technologies industrielles, Nathan, 2001.

Biographies

Dr. Loïc Andolfatto completed his doctoral studies in 2013 at École Normale Supérieure de Cachan and at the corporate research center Innovation Works of Airbus Group. He joined the EPFL Laboratory for Hydraulic Machines in 2014 as a research associate and worked on topics regarding modeling and optimization of hydraulic machine performance. He is now head of LMH Testing Team, which is providing independent testing of reduced scale physical models of hydraulic machines.

Danier Biner graduated in 2014 the Bachelor of Science in Systems Engineering, Design & Materials specialization, at the University of Applied Sciences Western Switzerland, HES-SO Valais-Wallis in Sion. Since September 2014, he is scientific assistant at the HES-SO Valais-Wallis, besides he is going through the MSE master's degree studies in industrial technologies at the HES-SO. His main research interests are the hydraulic design, the performance measurements, flow simulations and the optimization of small-scale hydro machinery.

Prof. Cécile Münch obtained an engineering degree from INPG, École Nationale Supérieure d'Hydraulique, Grenoble France ENSHMG in 2002. She completed her doctoral degree in 2005 on large eddy simulations of compressible turbulent flows. After working as a research associate in the Laboratory for Hydraulics Machines at EPFL until 2010, she is professor and head of a new hydraulic research team specialized in small hydro applications at the HES-SO Valais//Wallis, Switzerland.

Prof. François Avellan joined EPFL in 1984. He is director of the EPFL Laboratory for Hydraulic Machines since 1994 and he was appointed Ordinary Professor in 2003. His main research interests are the hydrodynamics of turbines, pumps and pump-turbines, including cavitation, hydro-acoustics, design and evaluation of the performance of hydraulic machines trough both experimental investigations and numerical simulations.